Safe Autonomous Overtaking with Intention Estimation

Vishnu S. Chipade[1], Qiang Shen[2], Lixing Huang[3], Necmiye Ozay[4,3], Sze Zheng Yong[2], Dimitra Panagou[1,3]

***Abstract*— This paper investigates the problem of overtaking a lead car by an autonomous ego car on a two-lane road in the presence of an oncoming car. We propose an intention-aware overtaking controller for the ego car. The intention of the lead car is estimated via a combination of active model discrimination and model selection algorithms. Then, a safe overtaking controller is designed based on vector fields that take into account the estimated intent, and ensure safety of the overtaking maneuver. Simulation results demonstrate the efficacy of the proposed approach.**

I. Introduction

Autonomous cars have been a very active topic of research recently due to numerous potential benefits such as driver comfort, reduced road fatalities, improved mobility, etc. Various aspects of them such as perception, real-time decision making and motion planning have been extensively studied (see, e.g., the review papers [1]–[4] for more details). In particular, safely overtaking a slower car moving on a two-lane road is of great interest since this could be crucial in emergency situations. Thus, in this paper, we investigate intent-aware safe overtaking of a lead car by an autonomous vehicle (the ego car) in the presence of an oncoming car on the left lane.

Autonomous overtaking has been studied using various strategies in the literature. The authors in [5] use MPC for generating overtaking trajectories in the presence of an oncoming car, while a hierarchical planning approach including strategic-level and low-level trajectory optimization for lane changing is presented in [6]. Receding horizon control has also been used to deal with lane changing problems, where the surrounding vehicles are modeled as Markov Gaussian Processes in [7], and stochastic MPC is employed to account for the uncertainty in other vehicles' motion. Similarly, the approach in [8] samples independent and identically distributed (iid) prediction trajectories of other vehicles from a generic model and build multi-level optimization problems based on these iid scenario samples. Other approaches use multi-policy decision making for high-level lane-changing behavior, where buffered Voronoi cells were used to compute a geometric partition and then, reducing the safety control design to ensuring that the vehicles avoid the partition boundaries [9]. However, these works do not consider the reaction of the other cars to the ego car's overtaking maneuver.

Another set of relevant literature pertains to approaches for active model discrimination, which injects a small input signal that causes the behaviors of all models to be distinct, thus can be discriminated from each other [10], [11]. These approaches have been successfully adopted for intention estimation in [12], [13]. In [12], an active model discrimination approach was proposed by solving an mixed-integer linear program (MILP) and applied to the problem of intention identification of other autonomous vehicle or human drivers in scenarios of intersection crossing and lane changing, while in [13], an affine abstraction-based separating input design problem was studied for a set of uncertain nonlinear models and used in an intention estimation example of a highway lane changing scenario with Dubins vehicle models.

In this paper, we propose a safe, autonomous overtaking algorithm for an ego car that accounts for the intention of a lead car. The intention estimation algorithm consists of two phases: 1) an offline phase where an optimal control input sequence for the ego car over a finite time horizon is found to distinguish the intentions of the lead car, and 2) an online phase where the computed sequence is applied to actively distinguish and find out the intention of the lead car. This intention is then used to generate an overtaking trajectory for the ego car, based on vector field guidance. The major contributions of this paper are: (1) the generalization of the active model discrimination formulation to allow piece-wise state-dependent constraints on the controlled inputs, making it applicable to a more general class of affine models when compared to those in [12], [13], and (2) an intent-aware, finite-time tracking controller for overtaking the lead car, based on a novel vector field guidance approach that uses super-elliptic contours and safely guides the ego car around the lead car.

The rest of the paper is organized as follows: Section II provides the mathematical modeling. The intent estimation, and trajectory generation and control algorithms are discussed in Sections III and IV, respectively. Simulation results are provided in Section VI. Conclusions and

[1]Department of Aerospace Engineering, University of Michigan, Ann Arbor, MI, USA; (vishnuc, dpanagou)@umich.edu

[2]School for Engineering of Matter, Transport and Energy, Arizona State University, Tempe, AZ, USA; (qiang.shen, szyong)@asu.edu

[3]Robotics Institute, University of Michigan, Ann Arbor, MI, USA; lixhuang@umich.edu

[4]Electrical Engineering and Computer Science Department, University of Michigan, Ann Arbor, MI, USA; necmiye@umich.edu

Toyota Research Institute (TRI) provided funds to assist the authors with their research but this article solely reflects the opinions and conclusions of its authors and not TRI or any other Toyota entity.

our thoughts on future work are provided in Section VII.

II. Modeling and Problem Statement

Notations: The set of positive integers up to n is denoted by $\mathbb{Z}_n^+$, and the set of non-negative integers up to n is denoted by $\mathbb{Z}_n^0$. Vectors are denoted in bold letters (e.g., $\mathbf{r}$). $\|\cdot\|$ is the 2-norm and $\|\cdot\|_\infty$ is the infinity vector norm.

A. Vehicle dynamics

We consider a two-lane road $\mathcal{R} \subseteq \mathbb{R}^2$ of lane width y_{lane}, and 3 cars: an ego car, $\mathcal{E}$, a lead car, $\mathcal{L}$, and an oncoming car, $\mathcal{O}$. All cars are identical in shape and are rectangular with length l_c and width $w_c (< y_{lane})$. The cars are assumed to have the following dynamics:

$$\dot{\mathbf{r}}_j = \begin{bmatrix} \dot{x}_j \\ \dot{y}_j \end{bmatrix} = \begin{bmatrix} v_{xj} \\ v_{yj} \end{bmatrix} = \mathbf{v}_j, \quad \dot{v}_{xj} = u_{xj} - C_d v_{xj}, \tag{1}$$

for $j \in \{e, l, o\}$. $\mathbf{r}_j = [x_j \ y_j]^\intercal$, for $j \in \{e, l, o\}$, are the position vectors of $\mathcal{E}$, $\mathcal{L}$ and $\mathcal{O}$, respectively, in the X-Y plane with respect to (w.r.t.) a global inertial frame $\mathcal{F}_g(\hat{\mathbf{i}}, \hat{\mathbf{j}}, \hat{\mathbf{k}})$ fixed on the outer edge of the rightmost lane as shown in Fig. 1; v_{xj} are longitudinal velocities; u_{xj} and v_{yj} are longitudinal acceleration inputs and lateral velocity inputs, respectively, which are bounded as:

$$|u_{xj}| \leq u_j^{max}, \ |v_{yj}| \leq v_j^{max}, \tag{2}$$

for $j = \{e, l, o\}$, and C_d is the coefficient of drag. Since overtaking requires more control authority for $\mathcal{E}$, we assume a larger control bound on $\mathcal{E}$ while overtaking:

$$|u_{xe}| \leq u_e^{max,over} \ . \tag{3}$$

This can be interpreted as that $\mathcal{E}$ will not fully utilize its control authority in normal driving, but in overtaking, it will leverage that to accomplish the task.

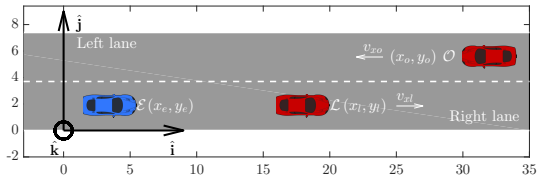

Fig. 1: Coordinate frame

The cars are modeled as rectangles with their edges aligned with the axes of $\mathcal{F}_g$, defined as:

$$\begin{aligned} \mathcal{E} &= \{\mathbf{r} \in \mathbb{R}^2 | \, |x - x_e| \leq \tfrac{l_c}{2}, |y - y_e| \leq \tfrac{w_c}{2}\}, \\ \mathcal{L} &= \{\mathbf{r} \in \mathbb{R}^2 | \, |x - x_l| \leq \tfrac{l_c}{2}, |y - y_l| \leq \tfrac{w_c}{2}\}, \\ \mathcal{O} &= \{\mathbf{r} \in \mathbb{R}^2 | \, |x - x_o| \leq \tfrac{l_c}{2}, |y - y_o| \leq \tfrac{w_c}{2}\}. \end{aligned} \tag{4}$$

For simplicity, we assume that $\mathcal{O}$ is moving with a constant speed v_{xo} on the left lane in the opposite direction.

B. Intention models of the lead car $\mathcal{L}$

During the intention estimation phase, we assume that $\mathcal{E}$ is behind $\mathcal{L}$ in the same lane and the headway $h(k) = x_l(k) - x_e(k)$ between $\mathcal{L}$ and $\mathcal{E}$ satisfies $h(k) > h_{min} > 0$ to avoid collision and ensure safety. We also limit our intention estimation problem to the case where $\mathcal{L}$ has a constant lateral position and its longitudinal velocity under different driving behaviors does not saturate in the process of intention estimation. Specifically, we consider two driver intentions $i \in \{A, C\}$ for $\mathcal{L}$, corresponding to Annoying and Cautious drivers, which are modeled as:

$$u_{xl,i} = \begin{cases} u_{xl,0} + K_{i,1}\Delta y + K_{i,2}\Delta h_i + \delta_i, & h_{min} < h < h_{max}, \\ u_{xl,0}, & \text{otherwise}, \end{cases} \tag{5}$$

where $\Delta y = y_e - y_l$, $\Delta h_A = h_{max} - h$, $\Delta h_C = h$, $K_{i,1}$ and $K_{i,2}$ are constants and δ_i is an input uncertainty accounting for nonlinear non-deterministic driving behavior. $u_{xl,0} = -K_0(v_{xl} - v_{xl}^{\text{des}}) + C_d v_{xl}^{\text{des}}$ is a baseline controller that represents the default lead car $\mathcal{L}$ behavior to maintain a desired speed v_{xl}^{des}. We choose $K_{A,1} > 0$ and $K_{A,2} > 0$ in (5) such that the annoying driver drives aggressively and speeds up when $\mathcal{E}$ tries to overtake $\mathcal{L}$, while $K_{C,1} < 0$ and $K_{C,2} < 0$ for the cautious driver who slows down and makes it easier for $\mathcal{E}$ to overtake $\mathcal{L}$.

C. Problem formulation

The problem of autonomously overtaking a lead car $\mathcal{L}$ in the presence of an oncoming car $\mathcal{O}$ on the left lane is hard task when there is no knowledge on how $\mathcal{L}$ is going to behave. Since the knowledge of $\mathcal{L}$'s intention would be beneficial in motion planning, we propose to split the overall overtaking problem into two sequential sub-problems: 1) Intent estimation of $\mathcal{L}$ based on the intent models (5), and 2) Overtaking control for $\mathcal{E}$ given the intention of $\mathcal{L}$. Formally, the sub-problems are:

***Problem** 1:* Estimate the intention of $\mathcal{L}$ over a fixed time horizon T. This includes the following two parts:

- *Active model discrimination:* Find an optimal $\mathcal{E}$'s input sequence $\boldsymbol{u}_T^* = \{\boldsymbol{u}_e^*(0), \ldots, \boldsymbol{u}_e^*(T-1)\}$ ($\boldsymbol{u}_e = [u_{xe} \ v_{ye}]^\intercal$, with zero-order hold) over a finite horizon T offline such that the observed trajectory of $\mathcal{L}$ is only consistent with one intention model regardless of any realization of uncertainties.
- *Model selection:* Implement the obtained optimal input sequence $\boldsymbol{u}_T^*$ alongside a model selection algorithm in real-time to identify the intention of $\mathcal{L}$ based on its observed output trajectories.

***Problem** 2:* Find a control input $\boldsymbol{u}_e = [u_{xe} \ v_{ye}]^\intercal$ for the ego car $\mathcal{E}$ to overtake the lead car $\mathcal{L}$ safely in the presence of the oncoming car $\mathcal{O}$ based on the estimated intention from Problem 1.

III. Intention Estimation of the Lead Car

In this section, we design an optimal $\mathcal{E}$'s input sequence and an intention estimation algorithm to distinguish the two intentions of $\mathcal{L}$. The following time-discretized model for $\mathcal{L}$ and $\mathcal{E}$ is used in this section:

$$v_{xe}(k+1) = (1 - C_d\Delta_T)v_{xe}(k) + u_{xe}(k)\Delta_T, \tag{6a}$$
$$y_e(k+1) = y_e(k) + v_{ye}(k)\Delta_T, \tag{6b}$$
$$h(k+1) = h(k) - v_{xe}(k)\Delta_T + v_{xl}(k)\Delta_T, \tag{6c}$$
$$v_{xl}(k+1) = (1 - C_d\Delta_T)v_{xl}(k) + u_{xl}(k)\Delta_T, \tag{6d}$$

where Δ_T is the sampling time. The output of the discrete-time model is $\mathcal{L}$'s velocity, i.e., $z_m(k) = v_{xl}(k)$. Note that the separating input $\boldsymbol{u}_e = [u_{xe} \ v_{ye}]^\intercal$ is equal for both intention models.

A. Vehicle dynamics with different intentions

The discrete-time state-space models $\mathcal{G}_i$, $i \in \{A, C\}$, for both the annoying car and cautious car, are given by

$$\vec{\boldsymbol{x}}_i(k+1) = A_i\vec{\boldsymbol{x}}_i(k) + B_i\boldsymbol{u}_e(k) + B_{\delta,i}\delta_i(k) + f_i, \quad (7)$$

$$z_i(k) = C_i\vec{\boldsymbol{x}}_i(k), \quad (8)$$

where $\vec{\boldsymbol{x}}_i(k) = [v_{xe,i}(k)\ y_{e,i}(k)\ h_i(k)\ v_{xl,i}(k)]^\intercal$, $z_i(k) = v_{xl,i}(k)$, and the system matrices are

$$A_i = \begin{bmatrix} 1 - C_d\Delta_T & 0 & 0 & 0 \\ 0 & 1 & 0 & 0 \\ -\Delta_T & 0 & 1 & \Delta_T \\ 0 & K_{i,1}\Delta_T & \overline{a}_i K_{i,2}\Delta_T & 1 - (K_0 + C_d)\Delta_T \end{bmatrix},$$

$$B_i = \begin{bmatrix} \Delta_T & 0 \\ 0 & \Delta_T \\ 0 & 0 \\ 0 & 0 \end{bmatrix}, B_{\delta,i} = \begin{bmatrix} 0 \\ 0 \\ 0 \\ \Delta_T \end{bmatrix}, f_i = \begin{bmatrix} 0 \\ 0 \\ 0 \\ (K_0 + C_d)v_{xl}^{\text{des}}\Delta_T + \overline{f}_i \end{bmatrix},$$

$C_i = \begin{bmatrix} 0\ 0\ 0\ 1 \end{bmatrix}$,

where $\overline{a}_i$ and $\overline{f}_i$ are defined as

$$\overline{a}_i = \begin{cases} -1, & i = A \\ 1, & i = C \end{cases}, \text{ and } \overline{f}_i = \begin{cases} K_{A,2}h_{max}\Delta_T, & i = A \\ 0, & i = C \end{cases}.$$

For both vehicle models $\mathcal{G}_i$, $i \in \{A, C\}$, we assume that the initial condition for model i, denoted by $\vec{\boldsymbol{x}}_i^0 = \vec{\boldsymbol{x}}_i(0)$, is constrained to a polyhedral set defined as:

$$\vec{\boldsymbol{x}}_i^0 \in \mathcal{X}_0 = \{\vec{\boldsymbol{x}} \in \mathbb{R}^4 : P_0\vec{\boldsymbol{x}} \le p_0\},\ \forall i \in \{A, C\}. \quad (9)$$

Further, the constraints on controlled input $\boldsymbol{u}_e$ in (2) are written using the following polyhedral set representation (for $k \in \mathbb{Z}_{T-1}^0$):

$$\boldsymbol{u}_e(k) \in \mathcal{U} = \{\boldsymbol{u}_e \in \mathbb{R}^2 : Q_u\boldsymbol{u}_e \le q_u\}. \quad (10)$$

In addition, $\mathcal{E}$'s lateral velocity input has to satisfy a piece-wise state-dependent constraint defined as

$$v_{ye} \in \begin{cases} \{0\}, & v_{xe,i} \in [v_e^{min}, v_{xe}^{dz}], \\ \{v_{ye} : \beta_1 \le \frac{v_{ye}}{(v_{xe,i} - v_{xe}^{dz})} \le \beta_2\}, & v_{xe,i} \in [v_{xe}^{dz}, v_e^{max}], \end{cases} \quad (11)$$

where v_{xe}^{dz} can be considered as a dead-zone, within which $\mathcal{E}$ does not have lateral motion, while β_1 and β_2 are slopes that mimic curvature constraints of real cars. The constraint in (11) implies that $\mathcal{E}$ is allowed to overtake $\mathcal{L}$ only when its longitudinal velocity is greater than v_{xe}^{dz}. An example of the piece-wise state-dependent constraint with $v_{xe}^{db} = 10$, $\beta_1 = -1$ and $\beta_1 = 1$ is shown in Fig. 2.

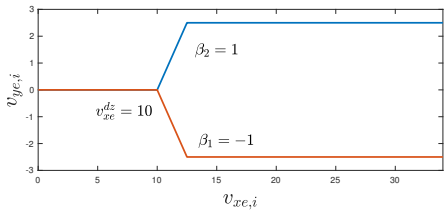

Fig. 2: Piece-wise state-dependent constraint in (11)

Moreover, the uncertainty δ_i is also constrained to a polyhedral set (for $k \in \mathbb{Z}_{T-1}^0$) defined as

$$\delta_i(k) \in \mathcal{D}_i = \{\delta \in \mathbb{R} : Q_{\delta,i}\delta \le q_{\delta,i}\}. \quad (12)$$

The states $\vec{\boldsymbol{x}}_i(k)$ are divided into controlled state $\boldsymbol{x}_i(k) = [v_{xe,i}(k)\ y_{e,i}(k)\ h_i(k)]^\intercal \in \mathbb{R}^3$ and uncontrolled state $y_i(k) = v_{xl,i}(k) \in \mathbb{R}$. The controlled state x_i are constrained to the following polyhedral set (for $k \in \mathbb{Z}_T^+$):

$$\boldsymbol{x}_i(k) \in \mathcal{X}_{x,i} = \{\boldsymbol{x} \in \mathbb{R}^3 : P_{x,i}\boldsymbol{x} \le p_{x,i}\}. \quad (13)$$

Specifically, we require $\mathcal{L}$ and $\mathcal{E}$ to keep a minimum distance to avoid collision during the intention estimation process, and this safety constraint is given by

$$h_i(k) \in \mathcal{H}_i = \{h \in \mathbb{R} : h \ge h_{min}\},$$

where $h_{min} > 0$ is a constant. We also constrain $\mathcal{E}$'s longitudinal velocity to an interval with $v_{xe,i} \in [v_e^{min}, v_e^{max}]$.

***Remark** 1:* We assume that the intention models are *well-posed*, whose definition can be found in [12, Remark 1]. Vehicle dynamic models are impractical if they are not well-posed, since the responsibilities of the inputs will be impossible to be satisfied.

Now, the Problem 1 can be formally redefined as:

***Problem** 3:* Given two intention models $\mathcal{G}_i$, $i \in \{A, C\}$, and state, input and uncertainty constraints, (9)-(11), find an optimal input $\boldsymbol{u}_T^* = \{\boldsymbol{u}_e^*(0), \ldots, \boldsymbol{u}_e^*(T-1)\}$ over a finite horizon T to minimize a given cost $\|\boldsymbol{u}_T\|_\infty$ ensuring comfort with small maximum input amplitudes, so that for all initial states $\vec{\boldsymbol{x}}_i(0)$ and uncertainty $\delta_i(k)$, $\forall k \in \mathbb{Z}_T^0$, only one model is valid, i.e., the output trajectories of models $\mathcal{G}_i$ over a finite horizon T have to differ by a separation threshold ϵ in at least one time instance. The optimization problem can be stated as:

$$\min_{\boldsymbol{u}_T, \boldsymbol{x}_{i,T}} \ \|\boldsymbol{u}_T\|_\infty$$

$$\text{s.t.} \quad \forall k \in \mathbb{Z}_{T-1}^0 : (10) \text{ holds}, \quad (14a)$$

$$\left.\begin{matrix} \forall i \in \{A, C\}, \\ \forall k \in \mathbb{Z}_T^0, \forall \vec{\boldsymbol{x}}_i^0, y_i(k), \delta_i(k) : \\ (7), (9), (12) \text{ hold} \end{matrix}\right\} : \begin{matrix} \forall k \in \mathbb{Z}_T^+ : \\ (11),\ (13) \text{ hold}, \end{matrix} \quad (14b)$$

$$\left.\begin{matrix} \forall i, j \in \{A, C\}, i \ne j, \\ \forall k \in \mathbb{Z}_T^0, \forall \vec{\boldsymbol{x}}_i^0, y_i(k), \delta_i(k) : \\ (7)\text{-}(8),\ (12)\text{-}(13) \text{ hold} \end{matrix}\right\} : \begin{matrix} \exists k \in \mathbb{Z}_T^0 : \\ |z_i(k) - z_j(k)| \ge \epsilon, \end{matrix} \quad (14c)$$

where $\boldsymbol{x}_{i,T} = \{\boldsymbol{x}_i(0), \ldots, \boldsymbol{x}_i(T)\}$ with $i \in \{A, C\}$.

B. Intention estimation approach

To solve Problem 1, an optimization-based approach is proposed, consisting of an offline active model discrimination step and an online model selection step. For brevity, we only give the main results of the approach. Its proofs are omitted as they follow similar steps to [12].

Proposition 1 (Active Model Discrimination): Given any separation threshold ϵ, the active model discrimination problem in Problem 3 is equivalent to a bilevel optimization problem with the following outer problem:

$$\min_{\boldsymbol{u}_T} \ \|\boldsymbol{u}_T\|_\infty \quad (P_{Outer})$$

$$\text{s.t.} \quad \forall k \in \mathbb{Z}_{T-1}^0 : (10) \text{ holds}, \quad (15a)$$

$$\left.\begin{matrix} \forall i \in \{A, C\}, \\ \forall k \in \mathbb{Z}_T^0, \forall \vec{\boldsymbol{x}}_i^0, y_i(k), \delta_i(k) : \\ (7), (9), (12) \text{ hold} \end{matrix}\right\} : \begin{matrix} \forall k \in \mathbb{Z}_T^+ : \\ (11),\ (13) \text{ hold}, \end{matrix} \quad (15b)$$

$$\Delta^*(\boldsymbol{u}_T) \ge \epsilon, \quad (15c)$$

where $\Delta^*(\boldsymbol{u}_T)$ is the solution to the inner problem:

$$\Delta^*(\boldsymbol{u}_T) = \min_{\Delta, \vec{\boldsymbol{x}}_i^0, \delta_{i,T}} \Delta \qquad (P_{Inner})$$

$$\text{s.t. } \forall i \in \{A, C\}, \forall k \in \mathbb{Z}_{T-1}^0 : (7),\ (12) \text{ hold}, \tag{16a}$$

$$\forall i \in \{A, C\}, \forall k \in \mathbb{Z}_{T}^0 : (8) \text{ holds}, \tag{16b}$$

$$\forall i \in \{A, C\} : (9) \text{ holds}, \tag{16c}$$

$$\left.\begin{matrix} \forall i, j \in \{A, C\}, i \neq j, \\ \forall k \in \mathbb{Z}_T^0 \end{matrix}\right\} : |z_i(k) - z_j(k)| \leq \Delta, \tag{16d}$$

where $\delta_{i,T} = \{\delta_i(0), \ldots, \delta_i(T)\}$ with $i \in \{A, C\}$.

Based on the bilevel problem proposed in Proposition 1, we can further leverage Karush-Kuhn-Tucker (KKT) conditions to convert the bi-level problem into a single level MILP problem, which can be solved by off-the-shelf optimization software, such as Gurobi [14] and CPLEX [15]. These details can be found in our previous paper [12, Theorem 1]. Comparing with [12], we consider additional piece-wise state-dependent constraints and responsibilities on the the controlled input in the outer problem of this paper, in order to make the intention estimation problem more realistic and practical.

In addition, to estimate the intention of $\mathcal{L}$, the optimal separating input is applied in real-time and the following model selection problem is considered:

Proposition 2 (Model Selection): Given two vehicle models $\mathcal{G}_i$, $i \in \{A, C\}$, and an input-output sequence $\{\boldsymbol{u}_e(k), z_m(k)\}_{k=0}^T$, where $\boldsymbol{u}_e(k)$ is obtained in Proposition 1, the model selection problem in Problem 1 is equivalent to the following feasibility problem:

$$\text{Find } \vec{\boldsymbol{x}}(k), \delta(k), i, \forall k \in \mathbb{Z}_{T-1}^0 \qquad (P_{MI})$$

$$\text{s.t.} \quad i \in \{A, C\},\ \forall k \in \mathbb{Z}_T^0 : z_m(k) - z_i(k) = 0,$$

$$\forall k \in \mathbb{Z}_{T-1}^0 : \vec{\boldsymbol{x}}(k+1) = A_i \vec{\boldsymbol{x}}(k) + B_i \boldsymbol{u}_e(k) + B_{\delta,i}\delta(k) + f_i,$$

$$(9) \text{ holds}, \forall k \in \mathbb{Z}_{T-1}^0 : (10)\text{-}(12) \text{ hold}, \forall k \in \mathbb{Z}_T^+ : (13) \text{ holds}.$$

We can solve the above feasibility check problem by leveraging the model invalidation algorithm in [16] and identify the true intention, which is guaranteed since the separating input in Proposition 1 is applied.

IV. Trajectory generation and control for the ego car

In this section, we provide a solution to Problem 2, i.e., we design the control actions $u_{xe}(t)$ and $v_{ye}(t)$ of $\mathcal{E}$ so that it safely overtakes $\mathcal{L}$ at some finite time $T < \infty$.

To assess the safety of the cars, we define a weighted ∞-norm distance between two rectangular cars i, j as:

$$\|\mathbf{r}_i - \mathbf{r}_j\|_{\bar{\infty}} = \max\left(\left|\frac{x_i - x_j}{l_c}\right|, \left|\frac{y_i - y_j}{w_c}\right|\right), \tag{18}$$

where l_c and w_c are the dimensions of the rectangles. The distance is referred to as ∞-distance hereafter.

***Definition** 1 (Safety):* Two cars i and j are safe with regards to each other if $\|\mathbf{r}_i(t) - \mathbf{r}_j(t)\|_{\bar{\infty}} > 1$, $\forall t \geq t_0$.

To ensure the safety of the ego car $\mathcal{E}$ from the lead car $\mathcal{L}$, we inflate $\mathcal{L}$ as $\bar{\mathcal{L}} = \{\mathbf{r} \in \mathbb{R}^2 \mid |x - x_l| \leq \frac{\bar{l}_c}{2}, |y - y_l| \leq \frac{\bar{w}_c}{2}\}$, where $\bar{l}_c = l_c + 2(x_{safe})$, $\bar{w}_c = w_c + 2(y_{safe})$, and $x_{safe} \geq \frac{l_c}{2}$, $y_{safe} \geq \frac{w_c}{2}$ are safety parameters. Further, let $R_l = \{y \in \mathbb{R} \mid \frac{w_c}{2} \leq y \leq y_{lane} - \frac{w_c}{2}\}$.

***Definition** 2 (Safe overtake):* A maneuver and the resulting trajectory $\mathbf{r}_e(t; t_0, \mathbf{r}_e(t_0))$ for $\mathcal{E}$, where the initial position of $\mathcal{E}$ is behind $\mathcal{L}$ on the same lane (i.e., $x_e(t_0) < x_l(t_0)$ and $y_e(t_0), y_l(t_0) \in R_l$) and its final position is ahead of $\mathcal{L}$ on the same lane (i.e., $x_e(t_f) > x_l(t_f)$ and $y_e(t_f), y_l(t_f) \in R_l$), is a safe overtake if $\mathcal{E}$ remains safe with regards to $\mathcal{L}$ and $\mathcal{O}$ (i.e., $\|\mathbf{r}_e(t) - \mathbf{r}_l(t)\|_{\bar{\infty}} > 1$ and $\|\mathbf{r}_e(t) - \mathbf{r}_o(t)\|_{\bar{\infty}} > 1$, $\forall t \in [t_o, t_f]$).

To enable safe overtake, we design a finite-time tracking controller based on a safe vector field. First, we choose a desired point $\mathbf{r}_d$ ahead of $\mathcal{L}$ that is subject to vehicle dynamics corresponding to the estimated intent from the previous section. Next, we define a vector field $\mathbf{F}$ that safely guides $\mathcal{E}$ around $\mathcal{L}$ to $\mathbf{r}_d$, and a tracking controller such that $\mathcal{E}$ tracks the vector field in finite-time.

The vector field $\mathbf{F}$ is a combination of two vector fields: (1) Guide-away vector field ($\mathbf{F}_l$), and (2) Guide-to vector field ($\mathbf{F}_d$). The Guide-away vector field $\mathbf{F}_l$ is defined to closely follow the rectangular shape of the cars using superquadric isopotential contours [17], called E-contours in this paper for brevity. The super-elliptic distance from $\mathcal{L}$ is defined as:

$$E_l(\mathbf{r}) = \left|\frac{x - x_l}{a}\right|^{2n} + \left|\frac{y - y_l}{b}\right|^{2n} - 1, \tag{19}$$

where $a = \frac{\bar{l}_c}{2}(2)^{\frac{1}{2n}}$, $b = \frac{\bar{w}_c}{2}(2)^{\frac{1}{2n}}$, $n > 1$, and is referred to as E-distance hereafter. For larger values of n, the contours corresponding to a constant value of E-distance E_l tend to be of rectangular shape. Figure 3 shows three contours for $E_l = 0$, $E_l = \bar{E}_l = 1.94$ and $E_l = E_l^u = 19.43$, with $n = 1.5$ and $\mathcal{L}$ situated at $[30, 1.85]^\intercal$.

The inflated lead car $\bar{\mathcal{L}}$ can be approximated by a bounding smallest super-ellipse that contains $\bar{\mathcal{L}}$: $\bar{\mathcal{L}}^m = \left\{\mathbf{r} \in \mathbb{R}^2 \mid E_l(\mathbf{r}) \leq 0\right\}$. Then, the slope of the tangent to E-contours at a point with position vector $\mathbf{r} \in \mathbb{R}^2$ is:

$$\tan(\bar{\beta}_l(\mathbf{r})) = -\frac{b^{2n}(x - x_l)\left|(x - x_l)\right|^{2n-2}}{a^{2n}(y - y_l)\left|(y - y_l)\right|^{2n-2}}. \tag{20}$$

Let the unit tangent vector at $\mathbf{r}$ be $\hat{\mathbf{t}}_l(\mathbf{r}) = \begin{bmatrix}\cos(\bar{\beta}_l(\mathbf{r}))\\ \sin(\bar{\beta}_l(\mathbf{r}))\end{bmatrix}$.

A. Vector fields for trajectory generation

1) Guide-away vector field: The Guide-away vector field $\mathbf{F}_l$ around the obstacle $\bar{\mathcal{L}}$ is defined as:

$$\mathbf{F}_l(\mathbf{r}) = \begin{bmatrix}\cos(\bar{\beta}_l'(\mathbf{r})) & \sin(\bar{\beta}_l'(\mathbf{r}))\end{bmatrix}^\intercal, \tag{21}$$

where $\beta_l'(\mathbf{r}) = \begin{cases}\bar{\beta}_l(\mathbf{r}) - \pi, & \left((\mathbf{r} - \mathbf{r}_d) \times \hat{\mathbf{t}}_l(\mathbf{r})\right) \cdot \hat{\mathbf{k}} > 0,\\ \beta_d - \pi, & \text{otherwise,}\end{cases}$

with $\beta_d = atan2\left(\frac{y - y_d}{x - x_d}\right)$. This way, $\mathbf{F}_l$ takes the form shown in regions $\mathcal{A}_l = \{\mathbf{r} \in \mathbb{R}^2 \mid 0 < E_l(\mathbf{r}) < \bar{E}_l, ((\mathbf{r} - \mathbf{r}_d) \times \hat{\mathbf{t}}_l(\mathbf{r})) \cdot \hat{\mathbf{k}} > 0\}$ (see violet vectors in Fig. 3) and $\mathcal{B}_l = \{\mathbf{r} \in \mathbb{R}^2 \mid 0 < E_l(\mathbf{r}) < E_l^u, ((\mathbf{r} - \mathbf{r}_d) \times \hat{\mathbf{t}}_l(\mathbf{r})) \cdot \hat{\mathbf{k}} \leq 0\}$ (see green vectors in Fig. 3).

2) Guide-to vector field: The Guide-to vector field $\mathbf{F}_d$ is defined as a radially converging vector field to the desired location $\mathbf{r}_d$:

$$\mathbf{F}_d(\mathbf{r}) = \frac{\mathbf{r}_d - \mathbf{r}}{\|\mathbf{r}_d - \mathbf{r}\|}. \tag{22}$$

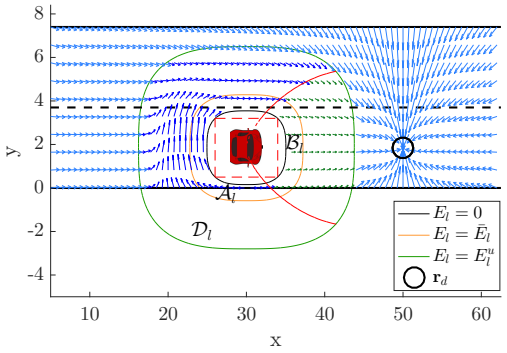

Fig. 3: Vector field definition around a rectangle

We set $\mathbf{F}_d(\mathbf{r}_d) = \mathbf{0}$, so that $\mathbf{F}_d$ is defined everywhere.

3) Combining vector fields: For the resulting vector field to be continuously differentiable near $\bar{\mathcal{L}}$, the Guide-to and Guide-away vector fields are combined using a blending function defined as:

$$\sigma(E_l) = \begin{cases} 1, & 0 \le E_l \le \bar{E}_l, \\ AE_l^3 + BE_l^2 + CE_l + D, & \bar{E}_l \le E_l \le E_l^u, \\ 0, & E_l^u \le E_l, \end{cases} \quad (23)$$

where $\bar{E}_l$, E_l^u are the super-elliptic distances defining the inner and outer boundaries of the blending region $\mathcal{D}_l = \{\mathbf{r} \in \mathbb{R}^2 \mid \bar{E}_l < E_l(\mathbf{r}) < E_l^u\}$, and the coefficients A, B, C, D are chosen as: $A = \frac{2}{(E_l^u - \bar{E}_l)^3}$, $B = \frac{-3(E_l^u + \bar{E}_l)}{(E_l^u - \bar{E}_l)^3}$, $C = \frac{6E_l^u \bar{E}_l}{(E_l^u - \bar{E}_l)^3}$, $D = \frac{(E_l^u)^2 (E_l^u - 3\bar{E}_l)}{(E_l^u - \bar{E}_l)^3}$, so that (23) is a $\mathcal{C}^1$ function. We choose $E_l^u = \left(\frac{2y_{lane} - \frac{w_c}{2} - y_l}{b}\right)^{2n} - 1$ such that $\mathbf{F}_l$ is active for $\frac{w_c}{2} \le y_e \le 2y_{lane} - \frac{w_c}{2}$. The value of $\bar{E}_l$ is chosen such that $\bar{E}_l < E_l^u$. The maximum distance x_{rep}^{max} from $\mathcal{E}$ along $\hat{\imath}$ at which the Guide-away vector field $\mathbf{F}_l$ is active is given as $x_{rep}^{max} = a\,(E_l^u + 1)^{\frac{1}{2n}}$. Then the Guide-to and Guide-away vector fields are blended as:

$$\mathbf{F} = (1 - \sigma(E_l))\mathbf{F}_d + \sigma(E_l)\mathbf{F}_l = [F_x \; F_y]^\intercal. \quad (24)$$

A vector field similar to $\mathbf{F}_l$ is considered around $\mathcal{O}$ when $\mathcal{E}$ attempts to overtake. However, the decision making and analysis is just based on the vector field around $\mathcal{L}$.

B. Control Design for the Ego Car

The desired position $\mathbf{r}_d$ of $\mathcal{E}$ is chosen ahead of $\mathcal{L}$ (i.e., $x_d(t) > x_l(t)$), and is assumed to follow dynamics:

$$\dot{\mathbf{r}}_d = \begin{bmatrix} \dot{x}_d \\ \dot{y}_d \end{bmatrix} = \begin{bmatrix} v_{xd} \\ v_{yd} \end{bmatrix} = \mathbf{v}_d, \quad \dot{v}_{xd} = u_{xd} - C_d v_{xd}, \quad (25)$$

where $v_{yd} = 0$, $u_{xd} = u_{xl,i0} + \delta_i^{min}$ and $u_{xl,i0} = u_{xl,i} - \delta_i$, $i = \{A,\ C,\ N\}$; $i = N$ stands for the case when $\mathcal{E}$ is not estimating the intention of $\mathcal{L}$, which we consider for comparison. In the latter case, $\mathcal{L}$ is assumed to be moving with constant average traffic speed (v_{tr}^{avg}), with some uncertainty in its acceleration such that the corresponding input is $u_{xl,N} = C_d v_{tr}^{avg} + \delta_N$, where $\delta_N \in [\delta_N^{min}, \delta_N^{max}]$.

We obtain the dynamics of the motion of $\mathcal{E}$ and $\mathcal{L}$ relative to a coordinate frame attached on $\mathbf{r}_d$. Define $\bar{\mathbf{r}}_e = \mathbf{r}_e - \mathbf{r}_d$, $\bar{\mathbf{v}}_e = \mathbf{v}_e - \mathbf{v}_d$ and $\hat{\mathbf{F}} = \frac{\mathbf{F}}{\|\mathbf{F}\|}$. Then the dynamics of $\mathcal{E}$ and $\mathcal{L}$ expressed in the new frame are:

$$\dot{\bar{\mathbf{r}}}_j = \begin{bmatrix} \dot{x}_j - \dot{x}_d \\ \dot{y}_j - \dot{y}_d \end{bmatrix} = \begin{bmatrix} v_{xj} - v_{xd} \\ v_{yj} - v_{yd} \end{bmatrix} = \bar{\mathbf{v}}_j, \quad \dot{\bar{v}}_{xj} = \bar{u}_{xj} - C_d \bar{v}_{xj}, \quad (26)$$

for $j \in \{e, l\}$, where $\bar{u}_{xe} = u_{xe} - u_{xd}$ and $\bar{u}_{xl} = u_{xl} - u_{xd} = \delta_i - \delta_i^{min}$. With this choice, we have that $\mathcal{L}$ is either stationary or moving towards the desired position $\mathbf{r}_d$. In the worst case, the maximum value of $\bar{u}_{xl}$ is $\bar{u}_{xl}^{max} = \delta_i^{max} - \delta_i^{min}$. This results in a maximum velocity of $\mathcal{L}$ relative to $\mathbf{r}_d$ of $\bar{v}_{xl}^{max} = \frac{\bar{u}_{xl}^{max}}{C_d}$.

We design a desired velocity profile for $\mathcal{E}$ that is safe and convergent to the desired position $\mathbf{r}_d$ along $\mathbf{F}$ as:

$$\bar{\mathbf{v}}_e^{des} = \begin{bmatrix} \bar{v}_{xe}^{des} \\ \bar{v}_{ye}^{des} \end{bmatrix} = \begin{cases} \hat{\mathbf{F}} k_r \|\bar{\mathbf{r}}_e\|^{\alpha_r}, & \|\bar{\mathbf{r}}_e\| \le R_e^f, \\ \hat{\mathbf{F}} \bar{v}_e^{over}, & \text{otherwise}, \end{cases}$$
$$\dot{\bar{\mathbf{v}}}_e^{des} = \begin{cases} \dot{\hat{\mathbf{F}}} k_r \|\bar{\mathbf{r}}_e\|^{\alpha_r} + k_r \alpha_r \hat{\mathbf{F}} \|\bar{\mathbf{r}}_e\|^{\alpha_r - 2} (\bar{\mathbf{r}}_e^\intercal \bar{\mathbf{v}}_e), & \|\bar{\mathbf{r}}_e\| < R_e^f, \\ \dot{\hat{\mathbf{F}}} \bar{v}_e^{over}, & \text{otherwise}, \end{cases} \quad (27)$$

where $\bar{v}_e^{over} > 0$ is a constant overtake speed, while $k_r > 0$ and $\alpha_r \in (0, 1)$ are chosen such that $\bar{v}_e^{over}$ is continuous during the overtake, $\bar{v}_e^{over} = k_r (R_e^f)^{\alpha_r}$, and R_e^f is the radius around the desired position where the finite-time convergent controller takes over.

We now propose the form of the tracking controllers for the control inputs u_{xe} and v_{ye} of $\mathcal{E}$. For the lateral velocity v_{ye} of $\mathcal{E}$, we define the control input as:

$$v_{ye} = \bar{v}_{ye}^{des} + v_{yd}, \quad (28)$$

where $\bar{v}_{ye}^{des}$ is the desired relative velocity along the y-axis. The acceleration input $\bar{u}_{xe}$ to track the desired longitudinal velocity $\bar{v}_{xe}^{des}$ is designed as:

$$\bar{u}_{xe} = C_d \bar{v}_{xe}^{des} + \dot{\bar{v}}_{xe}^{des} - k_v \bar{e}_{v_{xe}} |\bar{e}_{v_{xe}}|^{\alpha_v - 1}, \quad (29)$$

where $\bar{e}_{v_{xe}} = \bar{v}_{xe} - \bar{v}_{xe}^{des}$ and $\alpha_v \in (0, 1)$ is a gain. In the global coordinate frame, the input u_{xe} of $\mathcal{E}$ is:

$$u_{xe} = \bar{u}_{xe} + u_{xd}. \quad (30)$$

Theorem 1: The relative velocity $\bar{v}_{xe}$ converges to the desired relative velocity profile $\bar{v}_{xe}^{des}$ in finite time under the control action $\bar{u}_{xe}$ given by (29).

Proof: With $\bar{u}_{xe}$(Eq. (29)), the error dynamics is:

$$\dot{\bar{e}}_{v_{xe}} = -k_v \bar{e}_{v_{xe}} |\bar{e}_{v_{xe}}|^{\alpha_v - 1}. \quad (31)$$

From [18, Lemma 1], we obtain that the equilibrium $\bar{e}_{v_{xe}} = \bar{v}_{xe} - \bar{v}_{xe}^{des} = 0$ of (31) is finite-time stable. ■

The safe initial distance $|\bar{x}_l(t_0)|$ between $\mathcal{L}$ and $\mathbf{r}_d$ at the start of the overtake ($t = t_0$) should be such that $\mathcal{L}$ does not come $x_{rep}^{max} + R_e^f$ close to $\mathbf{r}_d$ when $\mathcal{E}$ converges to $\mathbf{r}_d$. Since the time of convergence T_f depends on $|\bar{x}_l(t_0)|$, we use an iterative approach to find $|\bar{x}_l(t_0)|$ as follows: Initialize $|\bar{x}_l(t_0)|_0 = x_{rep}^{max} + R_e^f$, then $|\bar{x}_l(t_0)|$ is iteratively updated using:

$$|\bar{x}_l(t_0)|_{m+1} = |\bar{x}_l(t_0)|_m + \|\bar{\mathbf{r}}_e(t_0 + \Delta t)\| \frac{\bar{v}_{xl}^{max}}{\bar{v}_e^{over}}, \quad (32)$$

where $\bar{v}_{xl}^{max}$ is the worst-case relative velocity, and $\Delta t = \frac{|\bar{x}_l(t_0)|_j - x_{rep}^{max} - R_e^f}{\bar{v}_{xl}^{max}}$. The iterative approach is terminated when $\|\bar{\mathbf{r}}_e(t_0 + \Delta t)\| < y_{lane} - \frac{w_c}{2} - y_d(t_0)$, where $y_d(t_0) =$

$y_e(t_0)$. This iterative approach is guaranteed to converge if $\bar{v}_{xl}^{max} < \bar{v}_e^{over}$ because after exiting $\mathcal{D}_l$, $\|\bar{\mathbf{r}}_e(t_0+\Delta t)\|$ is convergent to 0, which is discussed later. After $\mathcal{E}$ has successfully overtaken $\mathcal{L}$, $\mathcal{E}$ keeps tracking the desired position $\mathbf{r}_d$ that moves with a constant cruise speed v_e^{cr}.

C. Control Constraints

We want to design $\bar{v}_e^{over}$ such that the constraint in (3) is satisfied. Since $|u_{xd}| = \left|u_{xl,i0} + \delta_i^{min}\right| \leq u_l^{max}$ from (2), $\forall i = \{A, C, N\}$, we require $\bar{u}_{xe}$ to satisfy $\max(|\bar{u}_{xe}|) \leq u_e^{max,over} - u_l^{max}$, from (30). The overtaking maneuver constitutes of: (i) initially moving under the Guide-to vector field $\mathbf{F}_d$ until converging to the desired relative velocity (27), discussed later, (ii) entering the blending region $\mathcal{D}_l$, where $\bar{E}_l \leq E_l \leq E_l^u$, and (iii) entering the circular region $\{\mathbf{r}_e \in \mathbb{R}^2 | \, \|\mathbf{r}_e - \mathbf{r}_d\| \leq R_e^f\}$. The ego car has a constant relative speed $\bar{v}_e^{over}$ in the blending region, and the velocity vector $\bar{v}_{xe}$ is aligned with the vector field $\mathbf{F}$ before it enters the blending region. Then the acceleration $\bar{u}_{xe}$ is bounded as:

$$\bar{u}_{xe} \leq \begin{cases} |C_d \bar{v}_e^{over}| + \frac{k_r \bar{v}_e^{over}}{R_e^f}, & \|\bar{\mathbf{r}}_e\| < R_e^f, \\ |C_d \bar{v}_e^{over}| + \left|\dot{\bar{v}}_{xe}^{des}\right|, & \|\bar{\mathbf{r}}_e\| \geq R_e^f, \mathbf{r}_e \in \mathcal{D}_l, \\ |C_d \bar{v}_e^{over}| + \left|k_v \bar{e}_{v_{xe0}}^{\alpha_v}\right|, & \text{otherwise}, \end{cases} \tag{33}$$

where $\bar{e}_{v_{xe0}} \leq \bar{v}_e^{over}$, since $\mathcal{E}$ starts approaching $\mathcal{L}$ so it is moving at least as fast as $\mathcal{L}$.

Now, since $\dot{\bar{v}}_{xe}^{des} = \dot{\psi}_e \bar{v}_e^{over} \sin\psi_e \leq \bar{v}_e^{over} \left|\dot{\psi}_e\right|$, where $\psi_e = \tan^{-1}\left(\frac{F_y}{F_x}\right)$, the problem reduces to finding a bound on $\left|\dot{\psi}_e\right|$, and designing the velocity $\bar{v}_e^{over}$ such that it satisfies the overall control bound $\max(|\bar{u}_{xe}|) + u_l^{max} \leq u_e^{max,over}$.

Denote $\bar{F}_{v1} = \frac{[F_y \; -F_x]}{F_x^2+F_y^2} \begin{bmatrix} \frac{\partial F_x}{\partial \bar{x}_e} & \frac{\partial F_x}{\partial \bar{y}_e} \\ \frac{\partial F_y}{\partial \bar{x}_e} & \frac{\partial F_y}{\partial \bar{y}_e} \end{bmatrix} \frac{[Fx \; Fy]^T}{\sqrt{F_x^2+F_y^2}}$ and $\bar{\mathbf{F}}_{v2} = \frac{[F_y \; -F_x]}{F_x^2+F_y^2} \begin{bmatrix} \frac{\partial F_x}{\partial \bar{x}_l} & \frac{\partial F_x}{\partial \bar{y}_l} \\ \frac{\partial F_y}{\partial \bar{x}_l} & \frac{\partial F_y}{\partial \bar{y}_l} \end{bmatrix}$. The turning rate is then given as: $\dot{\psi}_e = \bar{F}_{v1} \bar{v}_e^{over} + \bar{\mathbf{F}}_{v2} \dot{\bar{\mathbf{r}}}_l \leq \left|\bar{F}_{v1}\right| \bar{v}_e^{over} + \left\|\bar{\mathbf{F}}_{v2}\right\| \left\|\dot{\bar{\mathbf{r}}}_l\right\|$. We consider the following problems:

$$\begin{aligned} &\max_{\bar{\mathbf{r}}_l \in D_s, \bar{\mathbf{r}}_e} \left|\bar{F}_{v1}\right| \; s.t. \; \bar{E}_l \leq E_l(\bar{r}_l, \bar{r}_e) \leq E_l^u, \\ &\max_{\bar{\mathbf{r}}_l \in D_s, \bar{\mathbf{r}}_e} \left\|\bar{\mathbf{F}}_{v2}\right\| \; s.t. \; \bar{E}_l \leq E_l(\bar{r}_l, \bar{r}_e) \leq E_l^u, \end{aligned} \tag{34}$$

where $D_s = \{(\bar{x}_l, \bar{y}_l) | \; |\bar{x}_l| \leq y_{lane} - \frac{w_c}{2}, \bar{y}_l \in [b_{min}, b_{max}]\}$ is a 2-D square region capturing that $\mathcal{L}$ stays in lane and maintains a bounded distance away from $\mathbf{r}_d$, and b_{min}, b_{max} are the search limits along the x-axis. Due to the non-convexity and non-linearity of these problems, we first search in the discretized 4-D space to obtain a point $(\bar{\mathbf{r}}_l^*, \bar{\mathbf{r}}_e^*)$ corresponding to a sub-optimal solution. We then optimize around the neighborhood $\mathcal{N}(\bar{\mathbf{r}}_l^*, \bar{\mathbf{r}}_e^*)$ of the sub-optimal solution:

$$\begin{aligned} &\max_{(\bar{\mathbf{r}}_l, \bar{\mathbf{r}}_e) \in \mathcal{N}(\bar{\mathbf{r}}_l^*, \bar{\mathbf{r}}_e^*)} \left|\bar{F}_{v1}\right| \; s.t. \; \bar{E}_l \leq E_l(\bar{r}_l, \bar{r}_e) \leq E_l^u, \bar{\mathbf{r}}_l \in D_s, \\ &\max_{(\bar{\mathbf{r}}_l, \bar{\mathbf{r}}_e) \in \mathcal{N}(\bar{\mathbf{r}}_l^*, \bar{\mathbf{r}}_e^*)} \left\|\bar{\mathbf{F}}_{v2}\right\| \; s.t. \; \bar{E}_l \leq E_l(\bar{r}_l, \bar{r}_e) \leq E_l^u, \bar{\mathbf{r}}_l \in D_s. \end{aligned} \tag{35}$$

Given the solutions $\bar{F}_{v1}^*$ and $\bar{\mathbf{F}}_{v2}^*$ to (35), we design $\bar{v}_e^{over}$ such that the maximum of the $\bar{u}_{xe}$ upper bounds in three phases described above satisfies the requirements: $u_l^{max} + \max\{(C_d + \frac{k_r}{R_e^f}), \; (C_d + \left\|\bar{\mathbf{F}}_{v2}^*\right\| \left\|\dot{\bar{\mathbf{r}}}_l\right\|) + \left|\bar{F}_{v1}^*\right| (\bar{v}_e^{over}), \; (C_d + k_v)\} \bar{v}_e^{over} \leq u_e^{max,over}$.

D. Safety and Convergence Analysis

To ensure that the relative velocity $\bar{\mathbf{v}}_e$ is aligned with $\bar{\mathbf{v}}_e^{des}$ when $\mathcal{E}$ enters the blending region $\mathcal{D}_l$, the overtaking starts with $\mathcal{E}$ at $x_e(t_0)$ such that $x_e(t_0) < x_l(t_0) - x_{rep}^{max} - x_c$, where x_c is the maximum bound on the distance that $\mathcal{E}$ would have traveled along $\hat{\mathbf{i}}$ relative to $\mathbf{r}_d$ before it converges to $\bar{\mathbf{v}}_e^{des}$. Integrating (31) yields: $\bar{e}_{v_{xe}}(t) = \bar{e}_{v_0}\left(1 - \frac{k_v(1-\alpha_v)t}{|\bar{e}_{v_0}|^{1-\alpha_v}}\right)^{\frac{1}{1-\alpha_v}}$, where $\bar{e}_{v_0} = \bar{e}_{v_{xe}}(0)$. The error $\bar{e}_{v_{xe}}(t)$ becomes 0 at $t = t_c = \frac{|\bar{e}_{v_0}|^{1-\alpha_v}}{k_v(1-\alpha_v)}$ and remains zero $\forall t \geq t_c$. Since $\bar{v}_{xe} \leq \bar{v}_e^{over}$, we have $x_c = t_c \bar{v}_e^{over}$.

Theorem 2: The position $\mathbf{r}_e(t)$ under the relative dynamics $\dot{\bar{\mathbf{r}}}_e = \bar{\mathbf{v}}_e^{des}$, where $\bar{\mathbf{v}}_e^{des}$ as in Eq. (27) is safe and convergent to $\mathbf{r}_d$ in some finite time T_f, if $\forall t < T_f$, $\mathbf{r}_d(t) \notin \mathcal{D}_l$, and $\min_{\mathbf{r} \in S_l} \|\mathbf{r}(t) - \mathbf{r}_d(t)\| > R_e^f$, where $\mathcal{S}_l = \{\mathbf{r} \in \mathbb{R}^2 \mid E_l(\mathbf{r}) = E_l^u\}$ is the boundary of $\mathcal{D}_l$.

Proof: By definition, $\bar{\mathbf{v}}_e^{des}$ is always aligned with $\mathbf{F}$, then showing $\mathbf{F}$ is safe implies $\bar{\mathbf{v}}_e^{des}$ is also safe. To show $\mathbf{F}$ is safe, we follow a similar analysis to [19, Lemma 1].

Consider $\mathcal{S}_l^- = \{\mathbf{r} \in \mathbb{R}^2 \mid E_l(\mathbf{r}) = E_l^u + \epsilon_E\}$ and $\mathcal{S}_l^+ = \{\mathbf{r} \in \mathbb{R}^2 \mid E_l(\mathbf{r}) = E_l^u - \epsilon_E\}$, with $\epsilon_E > 0$ arbitrarily small. Then:

$$\begin{aligned} \nabla S_l(\mathbf{r}) &= \left[\frac{2n}{x-x_l}\left|\frac{x-x_l}{a}\right|^{2n}, \frac{2n}{y-y_l}\left|\frac{y-y_l}{b}\right|^{2n}\right], \\ &= \nabla S_l^+(\mathbf{r}) = \nabla S_l^-(\mathbf{r}). \end{aligned} \tag{36}$$

From the definition of $\mathbf{F}$, we have: $\nabla S_l^- \mathbf{F} = \nabla S_l \mathbf{F}_d$, $\nabla S_l \mathbf{F} = \nabla S_l \mathbf{F}_d$. For $\nabla S_l^+ \mathbf{F}$, consider following cases:

1) Let $\mathbf{r} \in S^+$ s.t. $\left((\mathbf{r} - \mathbf{r}_d) \times \hat{\mathbf{t}}_l(\mathbf{r})\right) \cdot \hat{\mathbf{k}} > 0$, then by definition $\nabla S_l^+ \mathbf{F}_l = 0$. This implies that $\nabla S_l^+ \mathbf{F} = (1 - \sigma(E_l)) \nabla S_l^+ \mathbf{F}_d$. This gives us $(\nabla S_l^- \mathbf{F})(\nabla S_l^+ \mathbf{F}) > 0$, meaning that the integral curves cross the surface S_l. Let $\nabla S_l^+ \mathbf{F} > 0$, this implies $\nabla S_l \mathbf{F} > 0$. This contradicts the fact that the integral curves cross S_l. Then $\nabla S_l^+ \mathbf{F} < 0$, which means that the integral curves approach the boundary $T_l = \{\mathbf{r} \in \mathbb{R}^2 | E_l(\mathbf{r}) = \bar{E}_l\}$ of $\mathcal{D}_l$. Let $T_l^- = \{\mathbf{r} \in \mathbb{R}^2 | E_l(\mathbf{r}) = \bar{E}_l + \epsilon_E\}$. We have $\nabla T_l^- \mathbf{F} = \nabla S_l^+ \mathbf{F} < 0$ and $\nabla T_l \mathbf{F} = 0$ because on T_l we have $\sigma(\bar{E}_l) = 1$. This implies that the integral curves do not cross T_l and keep sliding over T_l until reaching $\mathcal{B}_l$. Since, by definition, the vector field $\mathbf{F}$ in $\mathcal{B}_l$ points toward $\mathbf{r}_d$ that is situated outside $\mathcal{B}_l$, one can show using a similar analysis that the integral curves exit $\mathcal{B}_l$.

2) $\left((\mathbf{r} - \mathbf{r}_d) \times \hat{\mathbf{t}}_l(\mathbf{r})\right) \cdot \hat{\mathbf{k}} \leq 0$. By definition, the vector fields $\mathbf{F}_l$ and $\mathbf{F}_d$ both point towards the desired location, which implies $\mathbf{F} = \mathbf{F}_d$. Then, using a similar analysis as in the previous case, it can be shown that the integral curves exit the switching surface S_l in this region.

This proves that $\mathbf{F}$ is safe and so is $\bar{\mathbf{v}}_e^{des}$. Now, since the blending region $\mathcal{D}_l$ is finite, the integral curves of $\mathbf{F}$ inside

$\mathcal{D}_l$ are of finite length. Then, an object moving with non-zero speed along the vector field $\mathbf{F}$ exits the blending region $\mathcal{D}_l$ in finite time. Further, we have that outside $\mathcal{D}_l$, the vector field $\mathbf{F}$ is convergent to $\mathbf{r}_d \notin \mathcal{D}_l$ by definition. Thus, given a non-zero speed and by moving along $\mathbf{F}$, there exists a finite time T_1 such that $\|\bar{\mathbf{r}}_e\| = R_e^f$. At this instance, $\hat{\mathbf{F}} = \frac{-\bar{\mathbf{r}}_e}{\|\bar{\mathbf{r}}_e\|}$ because $\sigma(E_l(\mathbf{r}_e)) = 0$. This renders the relative position dynamics as: $\dot{\bar{\mathbf{r}}}_e = -k_r \bar{\mathbf{r}}_e \|\bar{\mathbf{r}}_e\|^{\alpha_r - 1}$. The equilibrium $\mathbf{r}_e = \mathbf{r}_d$ of this system is finite-time stable as shown in [18, Lemma 1]. Let T_2 be time for $\bar{\mathbf{r}}_e(t)$ to converge to 0 with $\bar{\mathbf{r}}_e(0) = R_e^f$. Then, $\mathbf{r}_e$ converges to $\mathbf{r}_d$ in finite time $T_f = T_1 + T_2$ with $\bar{\mathbf{v}}_e = \bar{\mathbf{v}}_e^{des}$. ■

V. Overtake Decision Making

The ego car $\mathcal{E}$ is safe with respect to the lead car $\mathcal{L}$ as established in the previous section. The overtake is performed only when it is deemed safe with respect to the oncoming car $\mathcal{O}$. For the chosen $\mathbf{r}_d(t_0) = \begin{bmatrix} x_l(t_0) + |\bar{x}_l(t_0)| & y_e(t_0) \end{bmatrix}^\intercal$, we calculate the worst-case time and x-distance traveled by $\mathcal{E}$ before it overtakes $\mathcal{L}$, assuming maximum relative velocity of $\mathcal{L}$ relative to $\mathbf{r}_d$, i.e., $\bar{v}_{xl} = \bar{v}_{xl}^{max}$. Denote the worst-case time and x-distance by Δt_W and $\Delta x_{e,W}$, respectively, see Fig. 4, and the corresponding actual values as Δt and Δx_e.

For $\mathcal{E}$ to be safe with respect to $\mathcal{O}$, we require $\|\mathbf{r}_e(t) - \mathbf{r}_o(t)\|_{E_\infty} > 1$ for all $t \in [t_0, t_0 + \Delta t_W]$. Then, if $\mathbf{r}_o(t) \notin Z_1 = \{\mathbf{r}_o \in \mathbb{R} \mid x_e(t_0) < x_o(t) < x_e(t_0) + \Delta x_{e,W}\}$, we have $\|\mathbf{r}_e - \mathbf{r}_o\|_{E_\infty} > 1$, for all $t \in [t_0, t_0 + \Delta_W]$. For this to hold, $\mathcal{O}$ should start outside the region $Z_1 \cup Z_2$, shown in Fig. 4, so that $\mathcal{O}$ does not enter Z_1 during the worst-case overtake maneuver of $\mathcal{E}$, whose trajectory is denoted with the blue curve. This implies that $((x_o(t_0) - x_e(t_0)) > \Delta x_{e,W} + \Delta t_W\, |v_{xo}(t_0)|)$ OR $(x_o(t_0) < x_e(t_0))$, i.e., $\mathcal{O}$ requires at least Δt_W seconds to enter the unsafe zone Z_1 if it starts with $x_e(t_0) < x_o(t_0)$ OR it has already crossed Z_1 and thereby renders the overtake by $\mathcal{E}$ safe.

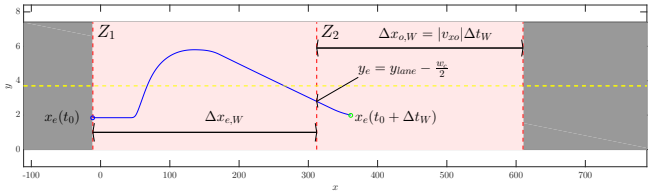

Fig. 4: Initial conditions of $\mathcal{O}$ for unsafe overtake

VI. Case Study and Simulation Results

We apply our proposed intention estimation based approach to the overtaking scenario when $\mathcal{E}$ is behind $\mathcal{L}$ in the same lane, where the underlying goal is to detect the intention of $\mathcal{L}$. Table I shows parameters of $\mathcal{L}$'s intention, while Table II depicts the initial conditions and state and input bounds used in this intention estimation step. The computed optimal input from Proposition 1 is $\boldsymbol{u}_e = \begin{bmatrix} 0 & 0 & 0 & 0 \\ 0.7919 & 0.7919 & 0 & 0 \end{bmatrix}$. Then, this optimal separating input is implemented in real-time while running the model selection algorithm in Proposition 2 to identify the intention of $\mathcal{L}$.

TABLE I: Parameters in intentions (5)

Parameter	Value	Parameter	Value	Parameter	Value
$K_{A,1}$	0.1	$K_{C,1}$	-0.5	δ_A	[-0.1,0.1]
$K_{A,2}$	0.002	$K_{C,2}$	-0.04	δ_C	[-0.1,0.1]
K_0	0.1	h_{min} $[m]$	4	h_{max} $[m]$	32

TABLE II: Initial conditions and parameters in intention estimation example

Parameter	Value	Parameter	Value
$v_{xe}(0)$ $[\frac{m}{s}]$	[22,26]	v_{xe} $[\frac{m}{s}]$	[0,34]
$y_e(0)$ $[m]$	[1.85,2.15]	y_e $[m]$	[0.9,2.8]
$h(0)$ $[m]$	[10,20]	v_{xl} $[\frac{m}{s}]$	[10,28]
$v_{xl}(0)$ $[\frac{m}{s}]$	[21,23]	$u_{xe}[\frac{m}{s^2}]$	[-4.2,4.2]
Δ_T $[s]$	0.25	v_{ye} $[\frac{m}{s}]$	[-2.5,2.5]
u_{xl} $[\frac{m}{s^2}]$	[-4.2,4.2]	v_{xl}^{des} $[\frac{m}{s}]$	22

Next, we provide simulation results for 3 case studies that demonstrate the efficacy of the proposed intention-aware overtaking algorithm for $\mathcal{E}$ in the presence of $\mathcal{O}$:

Case 1: The intention of $\mathcal{L}$ is not known (i.e., $i = N$). The control law for $\mathcal{E}$ is $u_{xd} = u_{xl,N0} + \delta_N^{min} = C_d v_{tr}^{avg} + \delta_N^{min}$.

Case 2: The intention of $\mathcal{L}$ is known and the driver is cautious (i.e., $i = C$), then $u_{xd} = u_{xl,C0} + \delta_C^{min}$.

Case 3: The intention of $\mathcal{L}$ is known and the driver is annoying (i.e., $i = A$), then $u_{xd} = u_{xl,A0} + \delta_A^{min}$.

Table IV shows Δt, Δx, Δt_W, Δx_W and the cumulative control effort during the overtake, $U = \int_{t_0}^{t_0+\Delta t} u_{xe} dt$ for the 3 cases with the initial conditions for $\mathcal{E}$, $\mathcal{L}$, $\mathcal{O}$ as given in Table III. It can be observed that, when there is no estimation of the intention of $\mathcal{L}$, then it is deemed unsafe for $\mathcal{E}$ to overtake for the given initial conditions. However, if $\mathcal{E}$ estimates the intention as in Cases 2 and 3, then overtaking is deemed safe. Additionally, when the $\mathcal{L}$'s driver is cautious, the x-distance that $\mathcal{E}$ traveled to overtake $\mathcal{L}$ and the control effort during the overtake U is smaller than the corresponding values when the $\mathcal{L}$'s driver is annoying. This is expected because the cautious driver slows down to ease out the overtaking maneuver of $\mathcal{E}$. Intention estimation helps in effectively deciding whether to overtake or not, and also in guiding $\mathcal{E}$ smoothly to overtake $\mathcal{L}$ in the presence of $\mathcal{O}$.

Fig. 5(a)–(b) show the ∞-distances between $\mathcal{E}$ and $\mathcal{L}$, and between $\mathcal{E}$ and $\mathcal{O}$, respectively, for the Case 3 when $\mathcal{L}$'s driver is annoying. As observed in Fig. 5(a)–(b), the ∞-distances are always greater than 1, demonstrating that there is no collision between $\mathcal{E}$ and the other two cars. Figure 6(a) shows the 2-norm distance between $\mathcal{E}$ and $\mathbf{r}_d$, which goes to zero in finite time, and hence $\mathcal{E}$ converges to the desired dynamics (25) in finite time. Moreover, Fig. 6(b) shows that control input u_{xe} applied by $\mathcal{E}$ is within the control bounds for all times. The discontinuities in u_{xe} at some places are because the desired velocity profile is only continuous and not differentiable at those points. The corresponding simulation video can be found at `https://youtu.be/fVyW3anBvC4`.

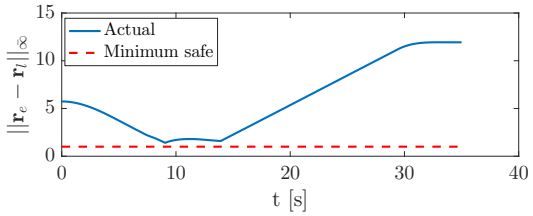

(a) Weighted ∞-norm distance between $\mathcal{E}$ and $\mathcal{L}$

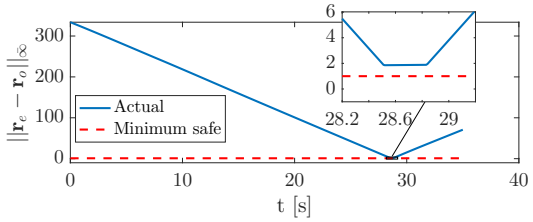

(b) Weighted ∞-norm distance between $\mathcal{E}$ and $\mathcal{O}$

Fig. 5: Weighted ∞-norm distances between the cars

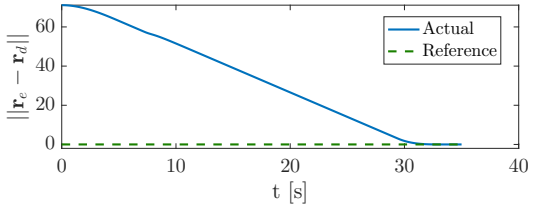

(a) 2-norm distance between $\mathcal{E}$ and $\mathbf{r}_d$

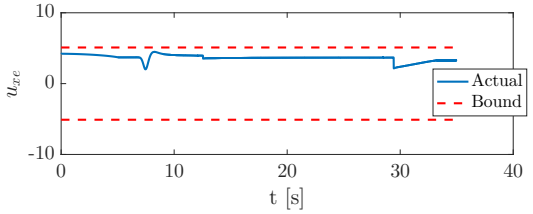

(b) Acceleration Input of $\mathcal{E}$

Fig. 6: Performance of the tracking controller

VII. Conclusions and Future Work

We developed an intention-aware overtaking algorithm using model discrimination and safe guidance techniques. The intention estimate enables the ego car to decide on whether it is safe to overtake a lead car. The guidance vector fields enable the safe overtake in the presence of an oncoming car. In the future, we would like to also include intention estimation for the oncoming car to further improve the overall proposed architecture.

References

[1] J. Van Brummelen, M. O'Brien, D. Gruyer, and H. Najjaran, "Autonomous vehicle perception: The technology of today and tomorrow," *Transportation research part C: emerging technologies*, 2018.

[2] W. Schwarting, J. Alonso-Mora, and D. Rus, "Planning and decision-making for autonomous vehicles," *Annual Review of Control, Robotics, and Autonomous Systems*, 2018.

[3] S. Lefèvre, D. Vasquez, and C. Laugier, "A survey on motion prediction and risk assessment for intelligent vehicles," *Robomech Journal*, vol. 1, no. 1, p. 1, 2014.

[4] C. Katrakazas, M. Quddus, W.-H. Chen, and L. Deka, "Real-time motion planning methods for autonomous on-road driving: State-of-the-art and future research directions," *Transportation Research Part C: Emerging Technologies*, vol. 60, pp. 416–442, 2015.

TABLE III: Initial conditions and other parameters

Initial Conditions				Other Parameters	
	$j=e$	$j=l$	$j=o$	Parameter	Value
$x_j(0)$ $[m]$	-22.96	0	835.19	$[\delta_N^{min}, \delta_N^{max}]$	[-0.15,0.15]
$y_j(0)$ $[m]$	1.85	2.8	5.55	$\bar{v}_e^{over}$	2.5
$v_{xj}(0)$ $[\frac{m}{s}]$	22	22	-22	R_e^f	3
				$\lvert u_e^{max,over} \rvert$	8.7

Road parameters							
y_{lane}	3.7	l_c	4	w_c	1.8	C_d	0.15

TABLE IV: Comparison of 3 cases ($x_o(t_0) - x_e(t_0) = 1335$)

Case (Intent)	$\Delta x_{e,W}[m]$ ($\Delta t_W[s]$)	$\Delta x_{o,W}[m]$	Is overtake safe?	$\Delta x_e[m]$ ($\Delta t[s]$)	U
1 (N)	1588.10 (65.45)	1439.90	No	-	-
2 (C)	650.14 (29.34)	645.48	Yes	559.97 (25.07)	86.30
3 (A)	714.86 (29.34)	645.48	Yes	616.23 (25.08)	94.98

[5] N. Murgovski and J. Sjöberg, "Predictive cruise control with autonomous overtaking," in *2015 IEEE 54th Conference on Decision and Control*, 2015, pp. 644–649.

[6] J. F. Fisac, E. Bronstein, E. Stefansson, D. Sadigh, S. S. Sastry, and A. D. Dragan, "Hierarchical game-theoretic planning for autonomous vehicles," *arXiv:1810.05766*, 2018.

[7] A. Carvalho, Y. Gao, S. Lefevre, and F. Borrelli, "Stochastic predictive control of autonomous vehicles in uncertain environments," in *12th Int. Sym. on Advanced Vehicle Control*, 2014.

[8] G. Cesari, G. Schildbach, A. Carvalho, and F. Borrelli, "Scenario model predictive control for lane change assistance and autonomous driving on highways," *IEEE Intelligent Transportation Systems Magazine*, vol. 9, no. 3, pp. 23–35, 2017.

[9] M. Wang, Z. Wang, S. Paudel, and M. Schwager, "Safe distributed lane change maneuvers for multiple autonomous vehicles using buffered input cells," in *2018 IEEE International Conference on Robotics and Automation*, May 2018, pp. 1–7.

[10] R. Nikoukhah and S. Campbell, "Auxiliary signal design for active failure detection in uncertain linear systems with a priori information," *Automatica*, vol. 42, no. 2, pp. 219–228, Feb. 2006.

[11] J. K. Scott, R. Findeison, R. D. Braatz, and D. M. Raimondo, "Input design for guaranteed fault diagnosis using zonotopes," *Automatica*, vol. 50, no. 6, pp. 1580–1589, Jun. 2014.

[12] Y. Ding, F. Harirchi, S. Z. Yong, E. Jacobsen, and N. Ozay, "Optimal input design for affine model discrimination with applications in intention-aware vehicles," in *ACM/IEEE International Conference on Cyber-Physical Systems*, 2018, available from: arXiv:1702.01112.

[13] K. Singh, Y. Ding, N. Ozay, and S. Z. Yong, "Input design for nonlinear model discrimination via affine abstraction," in *IFAC World Congress*, vol. 51, no. 16, 2018, pp. 175–180.

[14] Gurobi Optimization Inc., "Gurobi optimizer reference manual," 2015. [Online]. Available: http://www.gurobi.com

[15] IBM ILOG CPLEX, "V12. 1: User's manual for CPLEX," *Int. Business Machines Corporation*, vol. 46, no. 53, p. 157, 2009.

[16] F. Harirchi, S. Z. Yong, E. Jacobsen, and N. Ozay, "Active model discrimination with applications to fraud detection in smart buildings," in *IFAC World Congress*, vol. 50, no. 1, 2017, pp. 9527–9634.

[17] R. Volpe and P. Khosla, "Manipulator control with superquadric artificial potential functions: Theory and experiments," *IEEE Transactions on Systems, Man, and Cybernetics*, vol. 20, no. 6, pp. 1423–1436, 1990.

[18] K. Garg and D. Panagou, "New results on finite-time stability: Geometric conditions and finite-time controllers," in *2018 American Control Conference*, June 2018, pp. 442–447.

[19] D. Panagou, "A distributed feedback motion planning protocol for multiple unicycle agents of different classes," *IEEE Trans. on Automatic Control*, vol. 62, no. 3, pp. 1178–1193, 2017.